High-pressure Syntheses and Characterization of the Rare Earth Borates $RE_5(BO_3)_2F_9$ (RE = Dy, Ho)

Ernst Hinteregger, Gerhard Böhler, Thomas S. Hofer, and Hubert Huppertz

Institut für Allgemeine, Anorganische und Theoretische Chemie, Leopold-Franzens-Universität Innsbruck, Innrain 80 – 82, A-6020 Innsbruck, Austria

Reprint requests to H. Huppertz. E-mail: Hubert.Huppertz@uibk.ac.at

Z. Naturforsch. **2013**, *68b*, 29 – 38 / DOI: 10.5560/ZNB.2013-2313
Received November 26, 2012

The new rare earth fluoride borates $RE_5(BO_3)_2F_9$ (RE = Ho, Dy) were synthesized under high-pressure/high-temperature conditions of 1.5 GPa, 1250 °C for $Dy_5(BO_3)_2F_9$ and 2.5 GPa, 1200 °C for $Ho_5(BO_3)_2F_9$ in a Walker-type multianvil apparatus from the corresponding rare earth oxides, rare earth fluorides, and boron oxide. The single-crystal structure determinations have revealed that both compounds are isotypic to the known rare earth fluoride borates $RE_5(BO_3)_2F_9$ (RE = Er, Tm, Yb). The new fluoride borates crystallize monoclinically in the space group $C2/c$ ($Z = 4$) with the lattice parameters $a = 2046.7(4)$, $b = 615.9(2)$, $c = 829.6(2)$ pm, $\beta = 100.1(1)°$ for $Dy_5(BO_3)_2F_9$ and $a = 2039.5(4)$, $b = 612.7(2)$, $c = 827.1(2)$ pm, $\beta = 100.2(1)°$ for $Ho_5(BO_3)_2F_9$. Three crystallographically different nine-fold coordinated rare earth cations can be identified in the crystal structure. All boron atoms build up isolated trigonal-planar $[BO_3]^{3-}$ groups. In addition to the Raman and IR spectroscopic investigations, DFT-calculations were performed to support the assignment of the vibrational bands.

Key words: High Pressure, Fluoride, Borate, Crystal Structure, DFT

Introduction

The application of high-pressure/high-temperature techniques has led to a large variety of new fluoride borates. The first known compounds in the system *RE*-B-O-F were the rare earth fluoride borates $RE_3(BO_3)_2F_3$ (RE = Sm, Eu, Gd) [1, 2] and $Gd_2(BO_3)F_3$ [3]. They were synthesized by heating stoichiometric mixtures of RE_2O_3, B_2O_3 and REF_3 under ambient pressure. Under similar conditions, Kazmierczak *et al.* successfully synthesized the first divalent rare earth fluoride borate $Eu_5(BO_3)_3F$ [4], its structure being similar to the apatite type. Compared to the fluorapatite $Ca_5(PO_4)_3F$, the Eu^{2+} replace Ca^{2+} cations and the $[BO_3]^{3-}$ anions replace the phosphate tetrahedra. Up to now, high-temperature syntheses under ambient pressure conditions did not lead to any dysprosium or holmium fluoride borates. In the last years, a breakthrough was achieved in the system *RE*-B-O-F *via* high-pressure/high-temperature experiments leading to the compounds $Dy_3(BO_3)_2F_3$ [5], $Dy_4B_4O_{11}F_2$ [6] and $RE_2(BO_3)F_3$ (RE = Dy, Ho) [7], which are built up exclusively of isolated trigonal-planar $[BO_3]^{3-}$ groups. With the syntheses of the compounds $RE_5(BO_3)_2F_9$ (RE = Er – Yb) [8 – 10], three new rare earth fluoride borates were added to the known *RE*-B-O-F phases. The rare earth fluoride borates $RE_5(BO_3)_2F_9$ (RE = Dy, Ho) here reported are isotypic to these compounds. As a common trend in high-pressure borates, the boron atoms favor the four-fold coordination upon increasing pressure, so in most cases, the trigonal-planar $[BO_3]^{3-}$ groups transform into tetrahedral $[BO_4]^{5-}$ groups at pressures larger than 10 GPa. Above this pressure, only a few compounds containing trigonal-planar $[BO_3]^{3-}$ groups are known, *e. g.* $Ho_{31}O_{27}(BO_3)_3(BO_4)_6$ [11]. Because of the relatively mild pressure conditions, all boron atoms of the compounds $RE_5(BO_3)_2F_9$ (RE = Dy – Yb) are coordinated by three oxygen atoms. In the following, we describe the synthesis, the single-crystal structure determination, and IR/Raman spectroscopic investigations of $RE_5(BO_3)_2F_9$ (RE = Dy, Ho) as well as quantum-chemical calculations of harmonic vibrational frequencies of $Ho_5(BO_3)_2F_9$.

Experimental Section

Syntheses

According to Eqs. 1 and 2, the syntheses of the compounds $RE_5(BO_3)_2F_9$ (RE = Dy, Ho) were achieved under high-pressure/high-temperature conditions. For $Dy_5(BO_3)_2F_9$, the reaction was carried out at 1.5 GPa and 1250 °C, while the isotypic compound $Ho_5(BO_3)_2F_9$ was obtained at 2.5 GPa and 1200 °C.

$$Dy_2O_3 + B_2O_3 + 3\,DyF_3 \xrightarrow{1.5\ \text{GPa, } 1250\ ^\circ\text{C}} Dy_5(BO_3)_2F_9 \quad (1)$$

$$Ho_2O_3 + B_2O_3 + 3\,HoF_3 \xrightarrow{2.5\ \text{GPa, } 1200\ ^\circ\text{C}} Ho_5(BO_3)_2F_9 \quad (2)$$

Mixtures of Dy_2O_3 (Strem Chemicals, 99.9 %) or Ho_2O_3 (Strem Chemicals, 99.9 %), B_2O_3 (Strem Chemicals, 99.9+ %), and DyF_3 (Strem Chemicals, 99.9 %) or HoF_3 (Strem Chemicals, 99.9 %) with a molar ratio of 1 : 1 : 3 were finaly ground and filled into boron nitride crucibles (Henze BNP GmbH, HeBoSint® S100, Kempten/Germany). These crucibles were placed into the center of 18/11-assemblies. All working steps were done inside of a glove box. The 18/11-assemblies were compressed by eight tungsten carbide cubes (TSM-10 Ceratizit, Reutte/Austria). To apply the pressure, a 1000 t multianvil press with a Walker-type module (both devices from the company Voggenreiter, Mainleus/Germany) was used. The assembly and its preparation are described in refs. [12 – 16]. For the syntheses of $Dy_5(BO_3)_2F_9$/$Ho_5(BO_3)_2F_9$, the 18/11 assemblies were compressed up to 1.5/2.5 GPa in 45/65 min, then heated to 1250/1200 °C (cylindrical graphite furnace) within 10 min, kept there for 15 min, and cooled down to 450 °C in 25 min at constant pressure. After natural cooling down to room temperature by switching off the heating, decompression periods of 2/3.5 hours were required. The recovered octahedral pressure medium (MgO, Ceramic Substrates & Components Ltd., Newport, Isle of Wight/U.K.) was broken apart,

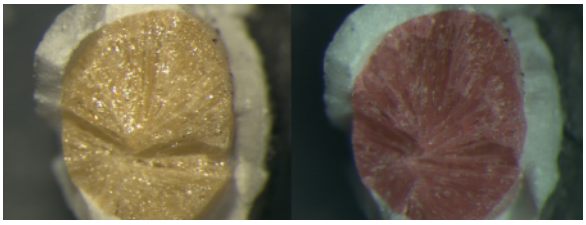

Fig. 1 (color online). Alexandrite effect of the compound $Ho_5(BO_3)_2F_9$ (left: daylight, right: incandescent light).

Table 1. Crystal data and structure refinement of $RE_5(BO_3)_2F_9$ (RE = Dy, Ho) (standard deviations in parentheses).

Empirical formula	$Dy_5(BO_3)_2F_9$	$Ho_5(BO_3)_2F_9$
Molar mass, g mol^{-1}	1101.12	1113.27
Crystal system	monoclinic	
Space group	$C2/c$ (no.15)	
Single crystal diffractometer	Enraf-Nonius Kappa CCD	
Radiation; wavelength, pm	Mo K_α; 71.073	
Single-crystal data		
a, pm	2046.7(4)	2039.5(4)
b, pm	615.9(2)	612.7(2)
c, pm	829.6(2)	827.1(2)
β, deg	100.1(1)	100.2(1)
V, Å^3	1029.3(4)	1017.1(4)
Formula units per cell, Z	4	
Calculated density, g cm^{-3}	7.11	7.27
Crystal size, mm^3	0.04 × 0.02 × 0.02	0.03 × 0.03 × 0.04
Temperature, K	293(2)	
Absorption coefficient, mm^{-1}	36.0	38.6
F(000), e	1876	1896
θ range, deg	2.0 – 37.8	2.0 – 37.8
Range in hkl	$-34 < h < 35$ $-10 < k < 9$ $-14 < l < 12$	$-34 < h < 34$ $-9 < k < 10$ $-14 < l < 12$
Total no. of reflections	7727	7820
Independent reflections / R_{int} / R_σ	2767 / 0.0777 / 0.0626	2731 / 0.0726 / 0.0578
Reflections with $I > 2\,\sigma(I)$	2569	2445
Data / ref. parameters	2767 / 102	2731 / 102
Absorption correction	multi-scan [17]	
Goodness-of-fit on F^2	1.077	1.084
Final $R1$ / $wR2$ [$I > 2\sigma(I)$]	0.0334 / 0.0860	0.0320 / 0.0759
$R1$ / $wR2$ (all data)	0.0363 / 0.0879	0.0370 / 0.0784
Largest diff. peak / hole, e Å^{-3}	4.66 / −5.12	4.13 / −4.40

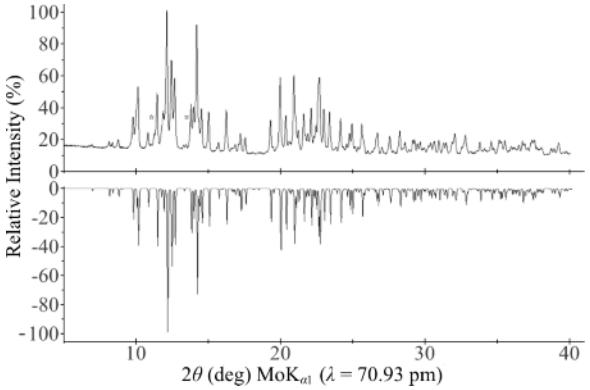

Fig. 2. Top: Experimental powder pattern of $Dy_5(BO_3)_2F_9$, reflections of an unknown phase are indicated with stars. Bottom: theoretical powder pattern of $Dy_5(BO_3)_2F_9$ simulated from single-crystal data.

and the samples were carefully separated from the surrounding graphite and boron nitride. While $Dy_5(BO_3)_2F_9$ was obtained in the form of light-green crystals, the compound $Ho_5(BO_3)_2F_9$ showed an intense alexandrite effect (daylight: yellow, incandescent light: pink) (Fig. 1). Both compounds are air-stable. All efforts to synthesize $RE_5(BO_3)_2F_9$ (RE = Dy, Ho) under ambient-pressure conditions were unsuccessful. The high-temperature syntheses were performed in boron nitride crucibles (Henze BNP GmbH, HeBoSint® S100, Kempten/Germany), which were placed into silica glass tubes. These assemblies were heated under ambient pressure conditions in a tube furnace from the company Carbolite.

Crystal structure analyses

The isotypic compounds $RE_5(BO_3)_2F_9$ (RE = Dy, Ho) were identified by powder X-ray diffraction on flat samples of the reaction products, using a Stoe Stadi P powder diffractometer with Mo$K_{\alpha 1}$ radiation (transmission geometry, Ge

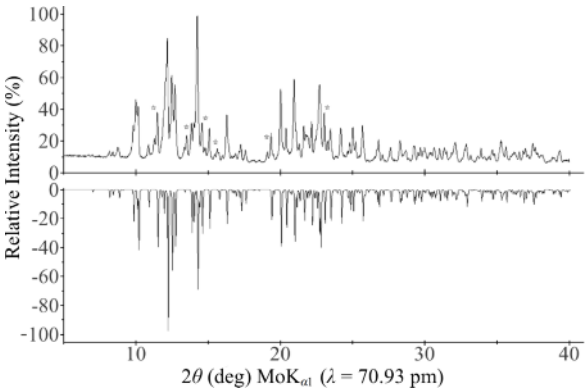

Fig. 3. Top: Experimental powder pattern of $Ho_5(BO_3)_2F_9$, reflections of an unknown phase are indicated with stars. Bottom: theoretical powder pattern of $Ho_5(BO_3)_2F_9$ simulated from single-crystal data.

Atom	Wyckoff position	x	y	z	U_{eq}
Dy1	8*f*	0.30614 (2)	0.11846(3)	0.18151(2)	0.00496(7)
Dy2	8*f*	0.39024(2)	0.38893(3)	0.59594(2)	0.00629(7)
Dy3	4*e*	1/2	0.10892(5)	1/4	0.00640(8)
B1	8*f*	0.3884(3)	0.9038(9)	0.4387(7)	0.0100(9)
O1	8*f*	0.4090(2)	0.7600(5)	0.5652(4)	0.0063(5)
O2	8*f*	0.3401(2)	0.0625(6)	0.4619(4)	0.0090(6)
O3	8*f*	0.4074(2)	0.1051(5)	0.7844(4)	0.0060(5)
F1	8*f*	0.2890(2)	0.4225(5)	0.0202(4)	0.0080(4)
F2	8*f*	0.3683(2)	0.4213(5)	0.3151(4)	0.0104(5)
F3	4*e*	1/2	0.4869(7)	1/4	0.0122(7)
F4	8*f*	0.2763(2)	0.7737(5)	0.2123(4)	0.0128(5)
F5	8*f*	0.4688(2)	0.1797(6)	0.5176(4)	0.0150(6)
Ho1	8*f*	0.30639(2)	0.11905(3)	0.18111(2)	0.00754(7)
Ho2	8*f*	0.39009(2)	0.38871(3)	0.59481(2)	0.00914(7)
Ho3	4*e*	1/2	0.10982(4)	1/4	0.00901(7)
B1	8*f*	0.3878(3)	0.9034(9)	0.4371(7)	0.0138(9)
O1	8*f*	0.4084(2)	0.7603(6)	0.5645(4)	0.0096(5)
O2	8*f*	0.3398(2)	0.0656(6)	0.4625(4)	0.0126(6)
O3	8*f*	0.4077(2)	0.1038(5)	0.7846(4)	0.0101(6)
F1	8*f*	0.2887(2)	0.4247(5)	0.0199(3)	0.0110(5)
F2	8*f*	0.3680(2)	0.4237(5)	0.3147(3)	0.0125(5)
F3	4*e*	1/2	0.4868(7)	1/4	0.0167(8)
F4	8*f*	0.2756(2)	0.7764(5)	0.2142(4)	0.0133(5)
F5	8*f*	0.4691(2)	0.1824(6)	0.5151(4)	0.0200(6)

Table 2. Atomic coordinates, Wyckoff positions, and equivalent isotropic displacement parameters U_{eq} (Å^2) of $RE_5(BO_3)_2F_9$ (RE = Dy, Ho) (space group: $C2/c$) with standard deviations in parentheses. U_{eq} is defined as one third of the trace of the orthogonalized U_{ij} tensor.

Table 3. Anisotropic displacement parameters of $RE_5(BO_3)_2F_9$ (RE = Dy, Ho) (space group: $C2/c$) with standard deviations in parentheses.

Atom	U_{11}	U_{22}	U_{33}	U_{23}	U_{13}	U_{12}
Dy1	0.0047(2)	0.0047(2)	0.0056(2)	−0.00015(5)	0.00130(7)	0.00027(5)
Dy2	0.0095(2)	0.0047(2)	0.0047(2)	−0.00026(5)	0.00142(7)	0.00204(6)
Dy3	0.0032(2)	0.0081(2)	0.0080(2)	0	0.00105(8)	0
B1	0.012(2)	0.011(2)	0.007(2)	−0.001(2)	0.002(2)	−0.0007(2)
O1	0.008(2)	0.005(2)	0.006(2)	0.0024(9)	0.0006(9)	−0.001(2)
O2	0.008(2)	0.015(2)	0.005(2)	0.002(2)	0.0033(9)	−0.005(2)
O3	0.006(2)	0.008(2)	0.004(2)	0.0002(9)	0.0011(9)	0.005(2)
F1	0.006(2)	0.008(2)	0.010(2)	0.0016(9)	0.0015(8)	0.001(2)
F2	0.015(2)	0.010(2)	0.007(2)	0.0006(9)	0.0028(9)	−0.003(2)
F3	0.011(2)	0.008(2)	0.018(2)	0	0.003(2)	0
F4	0.014(2)	0.011(2)	0.014(2)	0.001(2)	0.002(2)	−0.008(2)
F5	0.012(2)	0.016(2)	0.018(2)	−0.006(2)	0.006(2)	0.004(2)
Ho1	0.00733(9)	0.0058(2)	0.0095(2)	−0.00009(5)	0.00148(6)	0.00022(5)
Ho2	0.0130(2)	0.0060(2)	0.0084(2)	−0.00027(5)	0.00173(7)	0.00215(6)
Ho3	0.0059(2)	0.0093(2)	0.0119(2)	0	0.00154(9)	0
B1	0.014(2)	0.014(2)	0.013(2)	−0.002(2)	0.003(2)	−0.001(2)
O1	0.011(2)	0.008(2)	0.010(2)	0.002(2)	0.0014(9)	−0.002(2)
O2	0.009(2)	0.018(2)	0.009(2)	0.003(2)	−0.001(2)	−0.006(2)
O3	0.013(2)	0.010(2)	0.008(2)	0.000(2)	0.002(2)	0.003(2)
F1	0.008(2)	0.011(2)	0.014(2)	0.003(2)	0.0012(9)	0.0007(9)
F2	0.018(2)	0.009(2)	0.011(2)	0.001(2)	0.002(2)	−0.002(2)
F3	0.016(2)	0.012(2)	0.022(2)	0	0.004(2)	0
F4	0.012(2)	0.011(2)	0.017(2)	0.002(2)	0.0029(9)	−0.004(2)
F5	0.016(2)	0.021(2)	0.023(2)	−0.007(2)	0.006(2)	0.001(2)

monochromator, $\lambda = 70.93$ pm). Fig. 2 ($Dy_5(BO_3)_2F_9$) and Fig. 3 ($Ho_5(BO_3)_2F_9$) show the experimental powder patterns (top) that match well with the theoretical patterns (bottom) simulated from the single-crystal data. The respective diffraction patterns showed reflections of $Dy_5(BO_3)_2F_9$ or $Ho_5(BO_3)_2F_9$ and in both cases a still unknown side product (marked with stars in Figs. 2 and 3). Small single crystals of $Dy_5(BO_3)_2F_9$ and $Ho_5(BO_3)_2F_9$ were isolated by mechanical fragmentation. The single-crystal intensity data were collected at room temperature using a Nonius Kappa-CCD diffractometer with graphite-monochromatized Mo K_α radiation ($\lambda = 71.073$ pm). A semiempirical absorption correction based on equivalent and redundant intensities (SCALEPACK [17]) was applied to the intensity data. All relevant details of the data collection and evaluation are listed in Table 1 for both compounds. According to the systematic extinctions, the monoclinic space group $C2/c$ was derived in both cases. Due to the fact that the compounds $RE_5(BO_3)_2F_9$ (RE = Dy, Ho) are isotypic to $RE_5(BO_3)_2F_9$ (RE = Er – Yb) [8 – 10], the structural refinement was performed using the positional parameters of $Er_5(BO_3)_2F_9$ [9] as starting values (SHELXL-97 [18, 19] (full-matrix least-squares on F^2)). All atoms were refined with anisotropic displacement parameters, and the final difference Fourier syntheses did not reveal any significant peaks in both refinements. Tables 2 – 6 list the positional parameters, anisotropic displacement parameters, interatomic distances, and angles.

Further details of the crystal structure investigation may be obtained from the Fachinformationszentrum Karlsruhe, D-76344 Eggenstein-Leopoldshafen, Germany (fax: +49-7247-808-666; E-mail: crysdata@fiz-karlsruhe.de, http://www.fiz-informationsdienste.de/en/DB/icsd/depot_anforderung.html) on quoting the deposition numbers CSD-425427 and CSD-425428 for $Dy_5(BO_3)_2F_9$ and $Ho_5(BO_3)_2F_9$, respectively.

Vibrational spectra

The FTIR-ATR (*A*ttenuated *T*otal *R*eflection) spectra of powders were measured with a Bruker Alpha-P spectrometer with a diamond ATR-crystal (2×2 mm^2), equipped with a DTGS detector in the spectral range of 400 – 4000 cm^{-1} (spectral resolution 4 cm^{-1}). 24 scans of the sample were acquired. A correction for atmospheric influences using the OPUS 7.0 software was performed.

Confocal Raman spectra of single crystals of $Dy_5(BO_3)_2F_9$ were measured in the range of 150 – 4000 cm^{-1}, using a Horiba LABRAM HR-800 Raman micro-spectrometer under a 100 × objective (numerical aperture N.A. 0.9, Olympus, Hamburg, Germany). The crystal was excited by the 532.22 nm emission line of a 30 mW Nd:YAG laser (green). The laser focus on the sample surface was ∼1 μm. The scattered light was dispersed by a grating with 1800 lines/mm and collected by a 1024 × 256 open electrode CCD detector. Third order polynomial background subtraction, normalization, and band fitting by Gauss-Lorentz functions were done by the LABSPEC 5 software (Horiba). $Ho_5(BO_3)_2F_9$ showed a strong luminescence, which is typical for holmium-containing phases. Unfortunately, the strongest luminescence bands corresponded to the wavelengths of the common lasers used

for Raman spectroscopy (532 nm, 632 nm, and 785 nm). Therefore, it was not possible to distinguish between luminescence bands and real absorption bands, which made a characterization of $Ho_5(BO_3)_2F_9$ *via* Raman spectroscopy impossible.

DFT calculation

In addition to the experimentally recorded IR spectrum of $Ho_5(BO_3)_2F_9$, quantum-chemical computations of harmonic vibrational frequencies were performed using the CRYSTAL 09 program [20 – 22]. An important step of a quantum-mechanical calculation is the choice of an adequate basis set. A compromise had to be found between balancing computational effort and accuracy of the results. To reduce the computational effort, a basis set with an effective core potential (ECP) for holmium was chosen. A suitable basis set for the rare earth atom was identified based on geometry optimizations and calculations of harmonic vibrational frequencies of the high-pressure orthorhombic rare earth meta-oxoborate $Ho(BO_2)_3$ [23]. To consider the metastability of high-pressure modifications, the cell volume was kept constant during the geometry optimization. All-electron basis sets were employed for boron [24], oxygen [25], and fluorine [26]. Out of these results, the well tested ECP56MWB_GUESS [27, 28] basis set was chosen for the rare earth atoms. All calculations were performed with the PBESOL functional [29] for the correlation and exchange functional, and the SCF convergence for the energy was set to 10^{-12} E_h. The overall computation time for the calculations of harmonic vibrational frequencies of $Ho_5(BO_3)_2F_9$ took 12 weeks on a cluster with 16 Opteron dual-core 2.8 GHz processors.

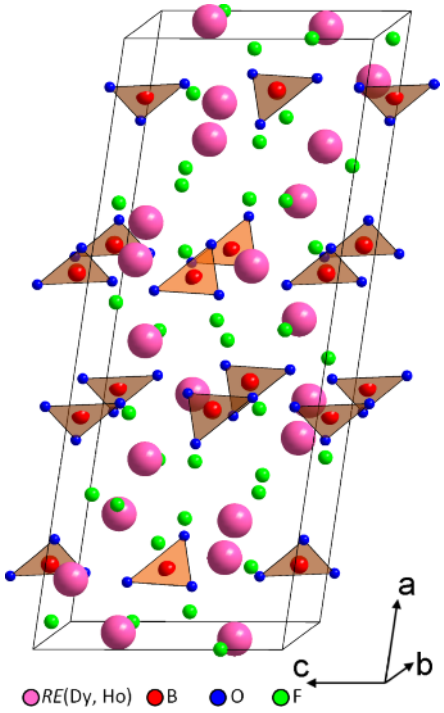

Fig. 4 (color online). Crystal structure of $RE_5(BO_3)_2F_9$ (RE = Dy, Ho) (space group: $C2/c$) showing isolated $[BO_3]^{3-}$ groups.

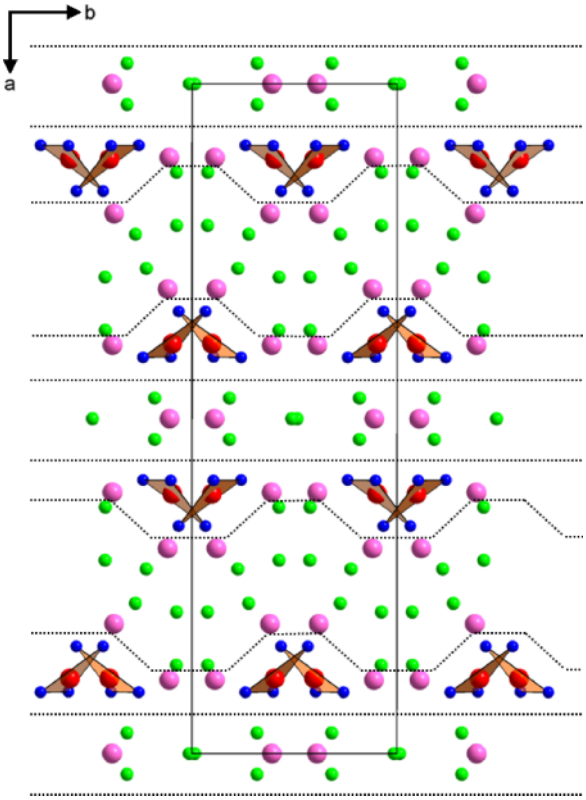

Fig. 5 (color online). Crystal structure of $RE_5(BO_3)_2F_9$ (RE = Dy, Ho) (space group: $C2/c$) depicting alternating layers in the bc plane with formal compositions 'REBO$_3$' and 'REF$_3$' (RE = Ho, Dy).

Results and Discussion

Crystal structure of $RE_5(BO_3)_2F_9$ (RE = Dy, Ho)

The crystal structures of $RE_5(BO_3)_2F_9$ (RE = Dy, Ho) consist of isolated trigonal $[BO_3]^{3-}$ anions, fluoride anions, and three crystallographically different rare earth cations (Fig. 4). Fig. 5 shows alternating layers of the formal compositions 'REBO$_3$' and

'REF$_3$' in the *bc* plane. Starting from $RE_3(BO_3)_2F_3$ (RE = Sm, Eu, Gd) [1, 2], the compound $RE_2(BO_3)F_3$ ($\equiv RE_3(BO_3)_2F_3 \cdot REF_3$ /2) (RE = Gd) [3] is formed by inserting a formal layer 'REF$_3$' into the *bc* plane. By adding a further layer 'REF$_3$' into the *bc* plane, $RE_5(BO_3)_2F_9$ ($\equiv RE_3(BO_3)_2F_3 \cdot 2\ REF_3$) ($RE$ = Dy – Yb) [8 – 10] is formed. For a detailed description of the structure, the reader is referred to the isotypic compounds $RE_5(BO_3)_2F_9$ [8 – 10]. In this paper, we briefly compare the isotypic phases $RE_5(BO_3)_2F_9$ (RE = Dy – Yb) and report the results of the DFT calculation. Table 4, 5 and 6 show the interatomic distances and angles for $Dy_5(BO_3)_2F_9$ and $Ho_5(BO_3)_2F_9$, respectively. The boron-oxygen distances inside the isolated trigonal $[BO_3]^{3-}$ groups are 138.1(6) – 142.7(7) pm with a mean value of 140.4 pm for $Dy_5(BO_3)_2F_9$ and 137.8(7) – 143.5(7) pm with a mean value of 140.2 pm for $Ho_5(BO_3)_2F_9$. The mean values of the boron-oxygen distances, ranging usually around 137 pm [30 – 32], are thus slightly larger. The RE–O/F (RE = Dy, Ho) distances range from 223.6(3) to 285.8(4) pm for $Dy_5(BO_3)_2F_9$ and from 222.2(3) to 287.6(3) pm for $Ho_5(BO_3)_2F_9$. The mean Ho–F distance in $Ho_5(BO_3)_2F_9$ (239.1 pm) is slightly shorter than the mean Dy–F distance in $Dy_5(BO_3)_2F_9$ (239.9 pm), which agrees with the size difference of the rare earth cations.

The charge distribution of the atoms in $RE_5(BO_3)_2F_9$ (RE = Dy, Ho) was also calculated *via* bond valence sums (ΣV) using VALIST (Bond Valence Calculation and Listing) [33] and *via* the CHARDI (*char*ge *di*stribution in solids) concept (ΣQ) [34 – 36], verifying the formal valence states in the fluoride borates. Table 7 shows the formal ionic charges, received from the calculations, which correspond to the expected values.

Furthermore, the MAPLE values (*MA*delung *P*art of *L*attice *E*nergy) [37 – 39] of $Dy_5(BO_3)_2F_9$ and $Ho_5(BO_3)_2F_9$ were calculated to compare them with the MAPLE values received from the summation of the binary components Dy_2O_3 [40], Ho_2O_3 [41], DyF_3 [42], HoF_3 [42], and the high-pressure modification B_2O_3-II [43]. The deviations between the products and the sum of the educts amount to 1.2 % for the dysprosium fluoride borate and to 0.9 % for $Ho_5(BO_3)_2F_9$.

Table 8 and Fig. 6 show the values of the lattice parameters of the isotypic compounds $RE_5(BO_3)_2F_9$ (RE = Dy – Yb). The differences correspond to the decreasing ionic radii of the ninefold coordinated rare earth ions (Dy^{3+} = 122.3, Ho^{3+} = 121.2, Er^{3+} = 120.2, Tm^{3+} = 119.2, and Yb^{3+} = 118.2 pm) [44], which is based on the lanthanide contraction. Due to the fact that the size difference is marginal, no greater deviations of the bond lengths and angles are

Dy1–O2a	233.3(3)	Dy2–O3	233.0(3)	Dy3–O1	233.8(3) (2×)
Dy1–O2b	234.3(3)	Dy2–O1	233.9(3)	Dy3–O3	236.6(3) (2×)
Dy1–O3	250.9(4)	Dy2–O2	243.5(4)	Dy3–F3	232.8(5)
Dy1–O1	257.6(4)	Dy2–F5	224.5(3)	Dy3–F5a	245.4(3) (2×)
Dy1–F4a	223.6(3)	Dy2–F2a	227.2(3)	Dy3–F5b	261.7(4) (2×)
Dy1–F4b	224.9(3)	Dy2–F2b	230.3(3)		
Dy1–F1a	229.3(3)	Dy2–F1	236.3(3)		
Dy1–F1b	234.6(3)	Dy2–F3	250.1(2)		
Dy1–F2	241.4(3)	Dy2–F4	285.8(4)		
	∅ = 236.7		∅ = 240.5		∅ = 243.1
B1–O1	138.1(6)				
B1–O3	140.3(7)				
B1–O2	142.7(7)				
	∅ = 140.4				
F1–Dy1a	229.3(3)	F2–Dy2a	227.2(3)	F3–Dy3	232.8(5)
F1–Dy1b	234.6(3)	F2–Dy2b	230.3(3)	F3–Dy2a	250.1(2) (2×)
F1–Dy2	236.3(3)	F2–Dy1	241.4(3)		
	∅ = 233.4		∅ = 233.0		∅ = 244.3
F4–Dy1a	223.6(3)	F5–Dy2	224.5(3)		
F4–Dy1b	224.9(3)	F5–Dy3a	245.4(3)		
F4–Dy2	285.8(4)	F5–Dy3b	261.7(4)		
	∅ = 244.8		∅ = 243.9		

Table 4. Interatomic distances (pm) in $Dy_5(BO_3)_2F_9$ (space group: $C2/c$) calculated with the single-crystal lattice parameters (standard deviations in parentheses).

observed. A closer look at the lattice parameters *a*, *b* and *c* reveals the anisotropy of the structure. Lattice parameter *b* rises more than the lattice parameters *a* and *c*.

Vibrational spectroscopy

The spectra of the FTIR-ATR measurements of $RE_5(BO_3)_2F_9$ (RE = Dy, Ho) are displayed in Fig. 7.

Table 5. Interatomic distances (pm) in $Ho_5(BO_3)_2F_9$ (space group: *C*2/*c*) calculated with the single-crystal lattice parameters (standard deviations in parentheses).

Ho1–O2a	232.9(3)	Ho2–O1	232.8(3)	Ho3–O1	233.7(3) (2×)
Ho1–O2b	233.5(3)	Ho2–O3	233.2(3)	Ho3–O3	235.1(4) (2×)
Ho1–O3	249.9(4)	Ho2–O2	240.2(4)	Ho3–F3	230.9(5)
Ho1–O1	255.3(3)	Ho2–F5	223.7(3)	Ho3–F5a	242.6(3) (2×)
Ho1–F4a	222.2(3)	Ho2–F2a	226.4(3)	Ho3–F5b	263.6(4) (2×)
Ho1–F4b	223.3(3)	Ho2–F2b	229.0(3)		
Ho1–F1a	229.0(3)	Ho2–F1	234.9(3)		
Ho1–F1b	233.4(3)	Ho2–F3	249.7(2)		
Ho1–F2	240.6(3)	Ho2–F4	287.6(3)		
	∅ = 235.6		∅ = 239.7		∅ = 242.3
B1–O1	137.8(7)				
B1–O3	139.3(7)				
B1–O2	143.5(7)				
	∅ = 140.2				
F1–Ho1a	229.0(3)	F2–Ho2a	226.4(3)	F3–Ho3	230.9(5)
F1–Ho1b	233.4(3)	F2–Ho2b	229.0(3)	F3–Ho2a	249.7(2) (2×)
F1–Ho2	234.9(3)	F2–Ho1	240.6(3)		
	∅ = 232.4		∅ = 232.0		∅ = 243.4
F4–Ho1a	222.2(3)	F5–Ho2	223.7(3)		
F4–Ho1b	223.3(3)	F5–Ho3a	242.6(3)		
F4–Ho2	287.6(3)	F5–Ho3b	263.6(4)		
	∅ = 244.4		∅ = 243.3		

Table 6. Interatomic angles (deg) in $RE_5(BO_3)_2F_9$ (RE = Dy, Ho) (space group: *C*2/*c*) calculated with the single-crystal lattice parameters (standard deviations in parentheses).

	O1–B1–O3	124.9(5)	Dy1a–F1–Dy1b	110.6(2)
	O1–B1–O2	117.5(4)	Dy1a–F1–Dy2	102.1(2)
	O3–B1–O2	117.4(4)	Dy1b–F1–Dy2	145.2(2)
		∅ = 119.9		∅ = 119.3
$Dy_5(BO_3)_2F_9$	Dy2a–F2–Dy2b	145.4(2)	Dy3–F3–Dy2a	107.8(2)
	Dy2a–F2–Dy1	101.1(2)	Dy3–F3–Dy2b	107.8(2)
	Dy2b–F2–Dy1	113.0(2)	Dy2a–F3–Dy2b	144.4(2)
		∅ = 119.8		∅ = 120.0
	Dy1a–F4–Dy1b	133.4(2)	Dy2–F5–Dy3a	132.7(2)
	Dy1a–F4–Dy2	92.2(2)	Dy2–F5–Dy3b	105.7(2)
	Dy1b–F4–Dy2	134.1(2)	Dy3a–F5–Dy3b	118.5(2)
		∅ = 119.9		∅ = 119.0
	O1–B1–O3	125.0(5)	Ho1a–F1–Ho1b	110.3(2)
	O1–B1–O2	116.9(4)	Ho1a–F1–Ho2	101.7(2)
	O3–B1–O2	118.1(4)	Ho1b–F1–Ho2	145.6(2)
		∅ = 120.0		∅ = 119.2
$Ho_5(BO_3)_2F_9$	Ho2a–F2–Ho2b	145.9(2)	Ho3–F3–Ho2a	107.8(2)
	Ho2a–F2–Ho1	100.8(2)	Ho3–F3–Ho2b	107.8(2)
	Ho2b–F2–Ho1	112.7(2)	Ho2a–F3–Ho2b	144.4(2)
		∅ = 119.8		∅ = 120.0
	Ho1a–F4–Ho1b	134.7(2)	Ho2–F5–Ho3a	133.3(2)
	Ho1a–F4–Ho2	91.5(2)	Ho2–F5–Ho3b	104.9(2)
	Ho1b–F4–Ho2	133.7(2)	Ho3a–F5–Ho3b	118.4(2)
		∅ = 120.0		∅ = 118.9

Table 7. Charge distribution in $RE_5(BO_3)_2F_9$ (RE = Dy, Ho) (space group: $C2/c$) calculated with VALIST (ΣV) [33] and the CHARDI concept (ΣQ) [34 – 36].

$Dy_5(BO_3)_2F_9$		Dy1	Dy2	Dy3	B1
	ΣV	3.19	2.99	2.82	2.75
	ΣQ	3.00	2.92	3.09	3.03
		O1	O2	O3	F1
	ΣV	−2.09	−2.08	−2.06	−0.99
	ΣQ	−2.05	−1.90	−1.98	−1.10
		F2	F3	F4	F5
	ΣV	−1.01	−0.75	−0.84	−0.81
	ΣQ	−1.15	−0.88	−0.93	−0.96
$Ho_5(BO_3)_2F_9$		Ho1	Ho2	Ho3	B1
	ΣV	3.16	2.96	2.79	2.76
	ΣQ	3.01	2.93	3.08	3.02
		O1	O2	O3	F1
	ΣV	−2.09	−2.07	−2.06	−0.98
	ΣQ	−2.05	−1.87	−2.01	−1.10
		F2	F3	F4	F5
	ΣV	−1.00	−0.75	−0.84	−0.80
	ΣQ	−1.14	−0.88	−0.93	−0.95

The assignments of the vibrational modes are based on a comparison with the experimental data of borates containing trigonal $[BO_3]^{3-}$ groups [45 – 47]. Absorption bands at 1200 – 1450 cm^{-1}, between 600 and 800 cm^{-1}, and below 500 cm^{-1} are expected for borates containing triangular $[BO_3]^{3-}$ groups.

In the FTIR spectra of $RE_5(BO_3)_2F_9$ (RE = Dy, Ho), the expected $[BO_3]^{3-}$ modes are detected between 1150 and 1450 cm^{-1} and between 600 and 800 cm^{-1}. If the 18/11 assembly was built up inside a glove box, no OH or water bands could be detected in the range of 3000 to 3600 cm^{-1}. Sample preparation outside the glove box led to O–H bands as described for $RE_5(BO_3)_2F_9$ (RE = Er, Tm) [9, 10]. A substitution of fluoride by hydroxyl groups can be assumed. For $RE_5(BO_3)_2F_9$ (RE = Dy, Ho), we could not notice a fluoride-hydroxide substitution.

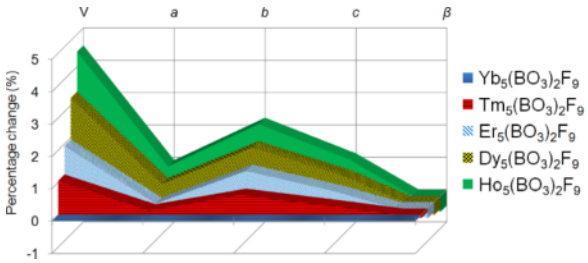

Fig. 6. Percentage change of the lattice parameters and volumes of the isotypic phases $RE_5(BO_3)_2F_9$ (RE = Dy, Ho, Er, Tm) relative to $Yb_5(BO_3)_2F_9$.

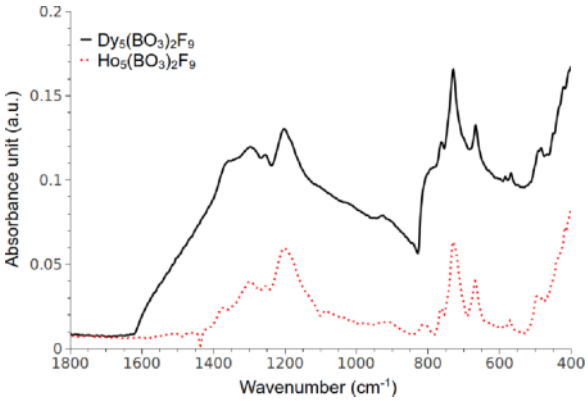

Fig. 7 (color online). Powder FT-IR reflectance spectra of $RE_5(BO_3)_2F_9$ [RE = Dy (black), Ho (red)] in the range 400 – 1800 cm^{-1}.

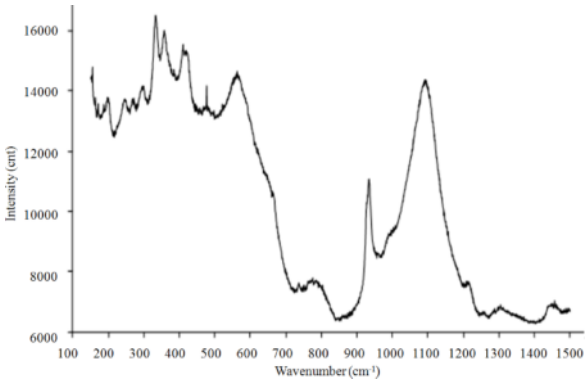

Fig. 8. Raman spectrum of a single crystal of $Dy_5(BO_3)_2F_9$ in the range 100 – 1500 cm^{-1}.

In order to complete the spectroscopic characterization, Raman measurements were performed on single crystals of $Dy_5(BO_3)_2F_9$. In Fig. 8, the Raman spectrum of $Dy_5(BO_3)_2F_9$ is shown. Bands below

	a	b	c	β	V	Reference
$Dy_5(BO_3)_2F_9$	2046.7(4)	615.9(2)	829.6(2)	100.1(1)	1029.3(4)	this work
$Ho_5(BO_3)_2F_9$	2039.5(4)	612.7(2)	827.1(2)	100.2(1)	1017.1(4)	this work
$Er_5(BO_3)_2F_9$	2031.2(4)	609.5(2)	824.6(2)	100.3(1)	1004.4(3)	[9]
$Tm_5(BO_3)_2F_9$	2030.9(4)	606.2(2)	822.6(2)	100.5(1)	995.7(3)	[10]
$Yb_5(BO_3)_2F_9$	2028.2(4)	602.5(2)	820.4(2)	100.6(1)	985.3(3)	[8]

Table 8. Comparison of the isotypic structures $RE_5(BO_3)_2F_9$ (RE = Dy, Ho, Er, Tm, Yb) (space group: $C2/c$).

Table 9. Theoretical IR bands in the spectrum of $Ho_5(BO_3)_2F_9$ (space group: $C2/c$).

Theoretical band	Assignment
1365	$s(B-O)_{BO_3}$
1295	$s(B-O)_{BO_3}$, $s(O-B-O)_{BO_3}$
1135	$s(B-O)_{BO_3}$, $b(O-B-O)$
1122	$s(B-O)_{BO_3}$, $s(O-B-O)_{BO_3}$
872	$s(B-O)_{BO_3}$
870	$s(B-O)_{BO_3}$
700	b(B – O – Ho)
699	b(B – O – Ho)
662	b(B – O – Ho)
648	b(O – B – O)
537	b(O – B – O)
502	s(F – Ho), s(F – Ho – F), s(Ho – O – Ho), s(Ho – O – B), b(B – O – Ho)
453	s(F – Ho), s(O – Ho – F), b(B – O – Ho), b(Ho – O – Ho)
442	s(F – Ho)
431	s(Ho – F – Ho), s(F – Ho)
416	s(O – Ho), b(Ho – O – Ho), b(O – Ho – F)
413	b(O – Ho – F), b(B – O – Ho), s(O – Ho)
395	s(Ho – F – Ho), b(Ho – F – Ho), s(F – Ho – F)
390	s(O – Ho), s(F – Ho), s(Ho – O – Ho), b(Ho – O – Ho)

s – stretching; b – bending; in brackets: pairs of bonded atoms with large relative motion between them; subscript BO_3 refer to the $[BO_3]^{3-}$ group in which the boron is located.

500 cm^{-1} can be interpreted by Dy–O / Dy–F bond bending and stretching as well as lattice vibrations. Modes above 1100 and around 900 and 500 cm^{-1} can be assigned to vibrations of $[BO_3]^{3-}$ groups [9, 10].

Density functional calculations of harmonic vibrational frequencies

Quantum-mechanical calculations of theoretical vibrational modes of large systems like $Ho_5(BO_3)_2F_9$ possessing several rare earth atoms are rarely found in literature. The calculation yielded 32 theoretically possible IR-active modes in the range 300 – 1500 cm^{-1}. The accuracy of the calculations and the quality of the results were acceptable to support the assignment of experimental vibrational bands. All calculated vibrational modes showed a shift. This deviation results from the approximations in the DFT method and the calculation of just a single unit cell. Calculations of larger systems (supercells) were not possible. Moreover, the calculation did not consider the temperature effects (297 K for the experiment). Unharmonicity and the superposition of two Gaussian peaks in the experimental spectrum led to a slight shift of the maxima.

The most intensive bands were evaluated and compared with the experimental spectrum, as listed in Table 9. As expected, in the region of higher wavenumbers the excitation occurred inside the trigonal $[BO_3]^{3-}$ groups as boron-oxygen stretching. The high variation of B–O distances inside the isolated BO_3 groups led to a large range (870 – 1365 cm^{-1}) for the B–O stretching modes. Bands at lower wavenumbers are more and more dominated by bending modes. In the region 650 – 750 cm^{-1} (calculated at 700, 699 and 662 cm^{-1}), the first bending mode of a boron-holmium-oxygen unit is observed. In the calculated spectrum, the first stretching vibrations of the type s(Ho–F) are located at 502 cm^{-1}, and those of the type s(Ho–O) at 416 cm^{-1}.

Conclusions

With the synthesis of $Dy_5(BO_3)_2F_9$ and $Ho_5(BO_3)_2F_9$, two new isotypic compounds in the series $RE_5(BO_3)_2F_9$ (RE = Dy, Ho, Er, Tm, Yb) were found and characterized. In accordance with the relatively mild applied pressures of 1.5 and 2.5 GPa, the structures consist exclusively of $[BO_3]^{3-}$ groups. To investigate the stability field of this structure type, additional experiments will be performed with the neighboring rare earth cations Tb^{3+} and Lu^{3+}.

Acknowledgement

We would like to thank Dr. G. Heymann for collecting the single-crystal data. The research was funded by the Austrian Science Fund (FWF): P 23212-N19.

[1] G. Corbel, R. Retoux, M. Leblanc, *J. Solid State Chem.* **1998**, *139*, 52.
[2] E. Antic-Fidancev, G. Corbel, N. Mercier, M. Leblanc, *J. Solid State Chem.* **2002**, *153*, 270.
[3] H. Müller-Bunz, Th. Schleid, *Z. Anorg. Allg. Chem.* **2002**, *628*, 2750.
[4] K. Kazmierczak, H. Höppe, *Eur. J. Inorg. Chem.* **2010**, *18*, 2678.
[5] A. Pitscheider, Dissertation, University of Innsbruck, Innsbruck (Austria) **2011**.
[6] A. Pitscheider, M. Enders, H. Huppertz, *Z. Naturforsch.* **2010**, *65b*, 1439.
[7] M. Enders, Diploma Thesis, University of Innsbruck, Innsbruck (Austria) **2011**.
[8] A. Haberer, H. Huppertz, *J. Solid State Chem.* **2009**, *182*, 888.
[9] A. Haberer, R. Kaindl, J. Konzett, R. Glaum, H. Huppertz, *Z. Anorg. Allg. Chem.* **2010**, *636*, 1326.
[10] A. Haberer, M. Enders, R. Kaindl, H. Huppertz, *Z. Naturforsch.* **2010**, *65b*, 1213.
[11] S. A. Hering, A. Haberer, R. Kaindl, H. Huppertz, *Solid State Sci.* **2010**, *12*, 1993.
[12] N. Kawai, S. Endo, *Rev. Sci. Instrum.* **1970**, *8*, 1178.
[13] D. Walker, M. A. Carpenter, C. M. Hitch, *Am. Mineral.* **1990**, *75*, 1020.
[14] D. Walker, *Am. Mineral.* **1991**, *76*, 1092.
[15] D. C. Rubie, *Phase Transitions* **1999**, *68*, 431.
[16] H. Huppertz, *Z. Kristallogr.* **2004**, *219*, 330.
[17] Z. Otwinowski, W. Minor in *Methods in Enzymology*, Vol. 276, *Macromolecular Crystallography*, Part A (Eds.: C. W. Carter Jr, R. M. Sweet), Academic Press, New York, **1997**, pp. 307.
[18] G. M. Sheldrick, SHELXS/L-97, Programs for Crystal Structure Determination, University of Göttingen, Göttingen (Germany) **1997**.
[19] G. M. Sheldrick, *Acta Crystallogr.* **2008**, *A46*, 112.
[20] R. Dovesi, V. R. Saunders, C. Roetti, R. Orlando, C. M. Zicovich-Wilson, E. Pascale, B. Civalleri, K. Doll, N. M. I. J. Bush, Ph. D'Arco, M. Llunell, CRYSTAL09, User's Manual, University of Torino, Torino (Italy), **2009**.
[21] R. Dovesi, R. Orlando, B. Civalleri, R. Roetti, V. R. Saunders, C. M. Zicovich-Wilson, *Z. Kristallogr.* **2005**, *220*, 571.
[22] F. Pascale, C. M. Zicovich-Wilson, F. Lopez, B. Civalleri, R. Orlando, R. Dovesi, *J. Comput. Chem.* **2004**, *25*, 888.
[23] H. Emme, T. Nikelski, Th. Schleid, R. Pöttgen, M. H. Möller, H. Huppertz, *Z. Naturforsch.* **2004**, *59*, 202.
[24] R. Orlando, R. Dovesi, C. Roetti, *J. Phys.: Condens. Matter* **1990**, *38*, 7769.
[25] L. Valenzano, F. J. Torres, K. Doll, F. Pascale, C. M. Zicovich-Wilson, R. Dovesi, *Z. Phys. Chem.* **2006**, *220*, 893.
[26] R. Nada, C. R. A. Catlow, C. Pisani, R. Orlando, *Modelling Simul. Mater. Sci. Eng.* **1993**, *1*, 165.
[27] M. Dolg, H. Stoll, A. Savin, H. Preuss, *Theor. Chim. Acta* **1989**, *75*, 173.
[28] M. Dolg, H. Stoll, H. Preuss, *Theor. Chim. Acta* **1993**, *85*, 441.
[29] J. P. Perdew, A. Ruzsinszky, G. I. Csonka, O. A. Vydrov, G. E. Scuseria, L. A. Constantin, X. Zhou, K. Burke, *Phys. Rev. Lett.* **2008**, *100*, 136406.
[30] E. Zobetz, *Z. Kristallogr.* **1990**, *191*, 45.
[31] F. C. Hawthorne, P. C. Burns, J. D. Grice in *Boron: Mineralogy, Petrology and Geochemistry*, (Ed.: E. S. Grew), Mineralogical Society of America, Washington, **1996**.
[32] E. Zobetz, *Z. Kristallogr.* **1982**, *160*, 81.
[33] A. S. Wills, VALIST (version 4.0.0), University College, London (U. K.) **1998**–**2008**; programm available from www.ccp14.ac.uk (retrieved December 10, 2012).
[34] I. D. Brown, D. Altermatt, *Acta Crystallogr.* **1985**, *B41*, 244.
[35] N. E. Brese, M. O'Keeffe, *Acta Crystallogr.* **1991**, *B47*, 192.
[36] R. Hoppe, S. Voigt, H. Glaum, J. Kissel, H. P. Müller, K. J. Bernet, *J. Less-Common Met.* **1989**, *156*, 105.
[37] R. Hoppe, *Angew. Chem., Int. Ed. Engl.* **1966**, *5*, 95.
[38] R. Hoppe, *Angew. Chem., Int. Ed. Engl.* **1970**, *9*, 25.
[39] R. Hübenthal, MAPLE (version 4), Program for the Calculation of MAPLE Values, University of Gießen, Gießen (Germany), **1993**.
[40] W. Hase, *Phys. Stat. Sol. B.* **1963**, *3*, 446.
[41] E. N. Maslen, V. A. Streltsov, N. Ishizawa, *Acta Crystallogr.* **1996**, *B24*, 869.
[42] A. Zalkin, D. H. Templeton, *J. Am. Chem. Soc.* **1953**, *75*, 2453.
[43] C. T. Prewitt, R. D. Shannon, *Acta Crystallogr.* **1968**, *B24*, 869.
[44] R. D. Shannon, *Acta Crystallogr.* **1976**, *A32*, 751.
[45] J. P. Laperches, P. Tarte, *Spectrochim. Acta* **1966**, *22*, 1201.
[46] H. Böhlhoff, U. Bambauer, W. Hoffmann, *Z. Kristallogr.* **1971**, *133*, 386.
[47] K. Machida, H. Hata, K. Okune, G. Adachi, J. Shiokawa, *J. Inorg. Nucl. Chem.* **1979**, *41*, 1425.